Exploring the Toxicity of a Bismuth–Asparagine Coordination Polymer on the Early Development of Zebrafish Embryos

ARTICLE *in* CHEMICAL RESEARCH IN TOXICOLOGY · DECEMBER 2012

Impact Factor: 3.53 · DOI: 10.1021/tx3004032 · Source: PubMed

8 AUTHORS, INCLUDING:

Xiang Li
Nankai University
11 PUBLICATIONS **25** CITATIONS
SEE PROFILE

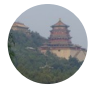

Dongyan Chen
Nankai University
19 PUBLICATIONS **77** CITATIONS
SEE PROFILE

Xi-Zeng Feng
Nankai University
53 PUBLICATIONS **761** CITATIONS
SEE PROFILE

Chemical Research in Toxicology

Article

pubs.acs.org/crt

Exploring the Toxicity of a Bismuth–Asparagine Coordination Polymer on the Early Development of Zebrafish Embryos

Ningning He,[†] Xiang Li,[‡] Daofu Feng,[†] Ming Wu,[‡] Rui Chen,[§] Tiehong Chen,[§] Dongyan Chen,*[,†] and Xizeng Feng*[,†,‡]

[†]The Key Laboratory of Animal Models and Degenerative Diseases, Department of Physiology, School of Medicine, Nankai University, Tianjin, 300071, China

[‡]State Key Laboratory of Medicinal Chemical Biology, Key Laboratory of Bioactive Materials, Ministry of Education, College of Life Science, Nankai University, Tianjin 300071, China

[§]Institute of New Catalytic Materials Science, Key Laboratory of Advanced Energy Materials Chemistry (MOE), College of Chemistry, Nankai University, Tianjin 300071, China

Supporting Information

ABSTRACT: Nanoparticles are widely used in nanomedicine, raising concerns about their toxicity. In this study, the toxicity of bismuth–asparagine coordination polymer spheres (BACP-2) was assessed in zebrafish embryos. Injection of 1–4 cell stage embryos with BACP-2 resulted in smaller head size (particularly smaller eye size), shorter body length, and pericardial edemas. The severity and occurrence of the resulting phenotype were concentration-dependent. The expression of genes such as *krox20*, orthodenticle homeobox 2 (*otx2*), and cardiac myosin light chain-2 (*cmlc2*) indicates that the effects of BACP-2 on the head and heart were related to changes in gene expression patterns. A delay in epiboly was observed, and the expression levels of the no tail (*ntl*) gene indicated that the delay in epiboly resulted both from the effect of BACP-2 on cell migration during epiboly and from slow growth. These findings indicate that BACP-2 exhibits concentration-dependent developmental toxicity, providing insight into the nanotoxicity of bismuth derivatives, which must be rigorously evaluated with respect to toxicity before their application in nanomedicine.

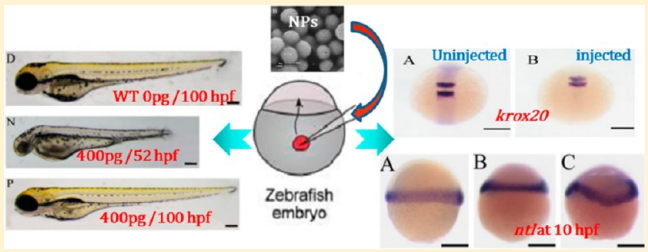

INTRODUCTION

Nanomaterials have undergone rapid development in recent years due to tremendous advances in synthesis and characterization techniques.[1,2] Nanomaterials are of interest because of their novel characteristics and applications. In spite of their merits in drug delivery, disease detection, and bioimaging, unpredictable side effects such as toxicity may be present. The specific toxicity and bioeffects of nanomaterials have become a major concern.

Multifunctional nanoscale coordination polymers have exhibited great potential for drug delivery, ion exchange, and multimodal bioimaging.[3−6] Although there are ongoing efforts to understand the potential effects of nanoscale coordination polymers (CPs), studies of bismuth-based nanostructured CPs are lacking. Although it is a heavy metal and transition ion, bismuth is considered to be relatively nontoxic. Several bismuth derivatives have been widely used in treatments for gastric and duodenal ulcers, diarrhea, and SARS.[7−9] Chen et al. synthesized bismuth–asparagine coordination polymer (BACP) nanostructures with diverse morphologies.[10] The BACPs exhibited passable biocompatibility *in vitro* and unique catalytic properties and biological interactions.[10] Luo et al. synthesized bismuth nanoparticles and reported toxicity higher than that previously reported *in vitro*.[11] However, the toxicity of bismuth-derived nanoparticles *in vivo* remains unclear.

The zebrafish (*Danio rerio*) has long been a promising animal model for developmental biology,[12−14] pharmacology,[15,16] and genetics[17,18] because of the unique advantages offered by this system, such as the strong similarity of its genome to the human genome and its rapid development with well-characterized developmental stages, easily observed transparent embryos, low-cost husbandry and housing, and high fecundity.[12−14] Zebrafish have recently been used in toxicity and biocompatibility assessments.[19−22] Wang et al. synthesized surface-enhanced Raman scattering (SERS) nanoprobes to detect the biocompatibility, toxicity, and biodistribution of nanoparticles in zebrafish.[21] Lee et al. synthesized Ag nanoparticles to investigate the transportation and biocompatibility of Ag nanoparticles in the developing zebrafish embryos.[23] In this article, bismuth–asparagine coordination polymer spheres (BACP-2) were used to study the toxicity and developmental effects of bismuth-derived nanoparticles in zebrafish embryos, in light of the toxicity of BACP-2 reported

Received: September 27, 2012
Published: December 21, 2012

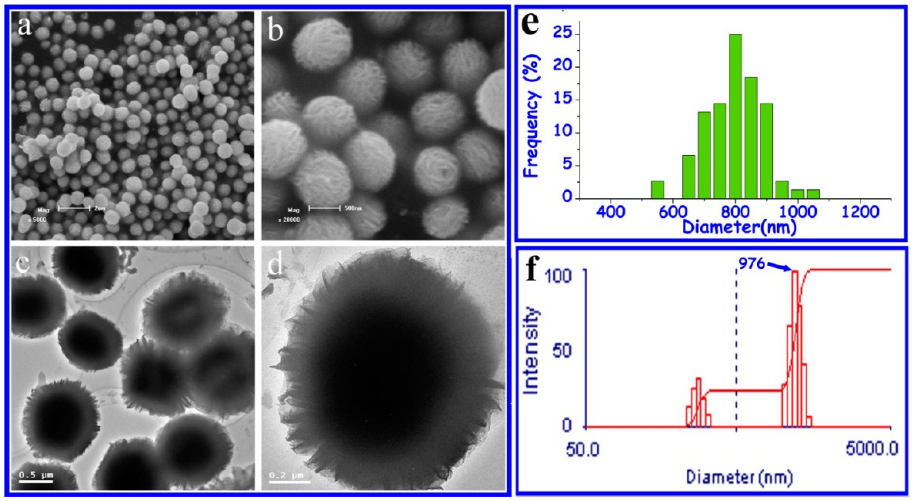

Figure 1. Morphological images of BACP-2 as acquired by SEM (a,b) and TEM (c,d). Diameter distribution (e) of BACP-2 by SEM and hydrodynamic diameters (f) of BACP-2 as measured by DLS.

by Chen et al.[10] The present article is, to our knowledge, the first concerning the toxicity and developmental effects of bismuth-derived nanoparticles in zebrafish embryos, used as a vertebrate model. The statistical analysis, morphology, and gene expression data indicate that BACP-2 possesses low developmental toxicity. However, this compound can result in the retardation of early embryonic development and problems in the expression of specific genes.

MATERIALS AND METHODS

Experimental Animals. The animals were maintained in aquaria at 28.5 °C with a 10/14-h dark/light cycle. All experimental protocols and procedures were performed in accordance with the NIH Guide for Care and Use of Laboratory Animals (No. 8023, revised 1996).

Nanoparticle Synthesis. BACP-2 was synthesized by adding bismuth nitrate ($Bi(NO_3)_3{\cdot}5H_2O$) to an asparagine solution. The solution was stirred until it became transparent, and the $Bi(NO_3)_3{\cdot}5H_2O$ and asparagine were reacted at 80 °C for 24 h to obtain well-dispersed submicrometer spheres (abbreviated as BACP-2) with an average diameter of approximately 800 nm.[8]

BACP-2 Characterization. The morphology of the products resulting from the hydrothermal treatment at 80 °C for 24 h (described above) was examined by scanning electron microscopy (SEM). The nanostructures were also characterized by transmission electron microscopy (TEM). To determine the size and distribution of BACP-2 in solution, hydrodynamic diameters were determined by dynamic light scattering (DLS).

Embryos and Microinjection. Adult wild-type zebrafish were maintained at 28.5 °C on a 14 h light/10 h dark cycle in standard system water (KCl 0.05 g L^{-1}, $NaHCO_3$ 0.025 g L^{-1}, NaCl 3.5 g L^{-1}, and $CaCl_2$ 0.1 g L^{-1}, pH 7.0–7.2). At the appropriate time for zebrafish mating, a ratio of one male to two females was established in one tank for maximum embryo production. The embryos were cultured at 28.5 °C in system water and staged as described.[24] Embryos at the two-cell stage were collected after natural spawning by visual assessment. Embryos at the two-cell stage were then transferred to the injection channel in an agarose plate with system water. Four nanoliters of BACP-2 (in double distilled water at concentrations of 0.0125, 0.05, and 0.1 g L^{-1}, respectively) or double distilled water (control group) was injected into the yolk of each embryo ($n > 40$). The quantities of BACP-2 that were injected into the embryos of the groups were 50 pg, 200 pg, and 400 pg. Embryos were then observed under a stereomicroscope for morphological analysis at different developmental stages from 6 h postfertilization (hpf) to 5 dpf for photography. Embryos at stages from 28 hpf to 100 hpf were dechorionated by forceps and anesthetized by immersion in tricaine for photographing under a stereomicroscope equipped with a digital camera. Head area and body length of embryos in control and BACP-2 injected groups were measured using the software of Olympus BP2-BSW at 28 hpf, 52 hpf, 76 hpf, and 100 hpf. Embryos in the control group and 400 pg of BACP-2 injected group were collected at 12 hpf (for *krox20* and *otx2*), at 24 hpf (for *cmlc2*), and at 33 hpf (for *cmlc2*) for *in situ* hybridization as well as at 5 dpf for alcian blue staining.

Whole-Mount *in Situ* Hybridization. Embryos were collected at the appropriate stages and fixed in 4% paraformaldehyde, pH 7.0, in phosphate-buffered saline overnight at 4 °C. Plasmids containing *ntl*, *krox20*, *otx2*, and *cmlc2* were generous gifts from Professor Hongwei Zhang (Shandong University). Digoxigenin (DIG)-labeled antisense RNA probes were transcribed with either SP6 or T7 RNA polymerases according to the manufacturer's instructions (Roche) using linearized plasmid as DNA templates. The embryos were dechorionated by forceps after washed three times with PBS and stored in methanol at −20 °C. Whole-mount *in situ* hybridization was performed as previously described.[25]

Alcian Blue Staining. Embryos were collected at 5 dpf and fixed in 4% paraformaldehyde (pH 7.0, in phosphate-buffered saline) overnight at 4 °C. Color cartilage staining was performed as previously described.[26]

RESULTS AND DISCUSSION

Synthesis and Characterization of BACP-2 Nanoparticles. BACP-2 was synthesized by adding bismuth nitrate ($Bi(NO_3)_3{\cdot}5H_2O$) to an asparagine solution and stirring the mixture until it became transparent. Well-dispersed submicrometer spheres (BACP-2) with an average diameter of approximately 800 nm were obtained by reaction of the mixed solution of $Bi(NO_3)_3{\cdot}5H_2O$, and asparagine was reacted at 80 °C for 24 h.[8] Then the morphology of the newly prepared products was examined by scanning electron microscopy (SEM) (Figure 1a,b). A large number of uniform sphere-like microstructures with an average size of 800 nm were formed (Figure 1a,b). More detailed morphological analysis (Figure 1b) revealed that the sphere-like structure was composed of abundant 2D nanoplates with thicknesses of approximately 500 nm. The nanostructures were further characterized by transmission electron microscopy (TEM) (Figure 1c,d). In agreement with SEM imaging, TEM imaging of the 3D sphere-like structures revealed that the entire particle was built from thin nanoplates. To determine the size and distribution of BACP-2 NPs in solution, hydrodynamic diameters were

dx.doi.org/10.1021/tx3004032 | Chem. Res. Toxicol. 2013, 26, 89–95

determined by DLS (Figure 1f). The average diameter of BACP-2 microspheres in solution was 976 nm. Two peaks were identified at 276 and 1168 nm by DLS, with a zeta potential of 40.9 mV (Table 1), yielding a diameter of BACP-2 dispersed in solution that was similar to that determined by TEM and SEM.

Table 1. Charactreristics of BACP-2 with Different Diameters

	D_n[a] (nm)	D_n[b] (nm)	zeta-potential (mV)
BACP-2	800	276,1168	+40.9

[a]From SEM characterization. [b]Hydrodynamic diameters determined by DLS.

Toxicity of BACP-2 Nanoparticles in Developing Zebrafish. To assess the toxicity of BACP-2 in zebrafish development, NPs of BACP-2 were microinjected into zebrafish embryos at the 1−4 cell stage, and the effects on the embryos were observed over the course of their development. BACP-2 was previously shown to exhibit concentration-dependent toxicity in 3T3 cells.[10] In this study, the toxicity of BACP-2 was evaluated at three different concentrations by observing the morphology of embryos that were injected with BACP-2 at different stages from 28 hpf to 100 hpf at 24-h intervals. At 28 hpf, embryos with smaller heads (particularly eyes) and shorter body lengths were observed in the groups that were injected with BACP-2 (Figure 2e,i,m). The percentages of embryos with smaller heads and shorter body lengths were 20%, 38%, 65%, and 77% in the groups that were injected with 0 pg, 50 pg, 200 pg, and 400 pg of BACP-2, respectively (Figure 2q). The abnormal phenotype was more severe in embryos injected with 200 pg and 400 pg of BACP-2 than in embryos injected with 50 pg of BACP-2 (Figure 2i,m,r,s). The percentage and severity of embryos with small heads and short body lengths in each group exhibited an obvious concentration dependence. Abnormal embryos from each group were then selected for developmental observation. At 52 hpf, the selected embryos continued to exhibit smaller head sizes and shorter body lengths (Figure 2b,f,j,n). The severity of the abnormal phenotype also remained dependent on the injected quantity of BACP-2. At 52 hpf, the BACP-2-injected embryos exhibited significant pericardial edema in comparison with that of uninjected embryos (Figure 2b,f,j,n), in addition to the defects in head size and body length. The percentages of embryos with pericardial edema were 50%, 57%, and 70% in the 50 pg, 200 pg, and 400 pg BACP-2-treated groups, respectively, demonstrating a clear dependence on BACP-2 concentration. Embryos with pericardial edema were not observed in the control (uninjected) group. The severity of pericardial edema increased as the amount injected into the embryos increased. At 76 hpf, the severity of pericardial edema in embryos injected with BACP-2 remained concentration-dependent (Figure 2c,j,k,o). The effects of BACP-2 on the head region and body length were not obvious at 28 hpf and 52 hpf (Figure 2c,g,k,o). At 100 hpf, no significant differences could be observed in the head region, body length, or pericardial edema among BACP-2-injected and uninjected embryos, suggesting that the embryos were able to recover to some extent from the effects of BACP-2 (Figure 2d,h,l,p). The severity and percentage of embryos with small head size, short body length, and pericardial edema in each group suggest that the effects of BACP-2 were significantly concentration-dependent.

At each concentration of BACP-2, observation of the morphological characteristics of the zebrafish embryos revealed the occurrence of a developmental delay from 50% epiboly stage to bud stage in embryos that were injected with BACP-2.

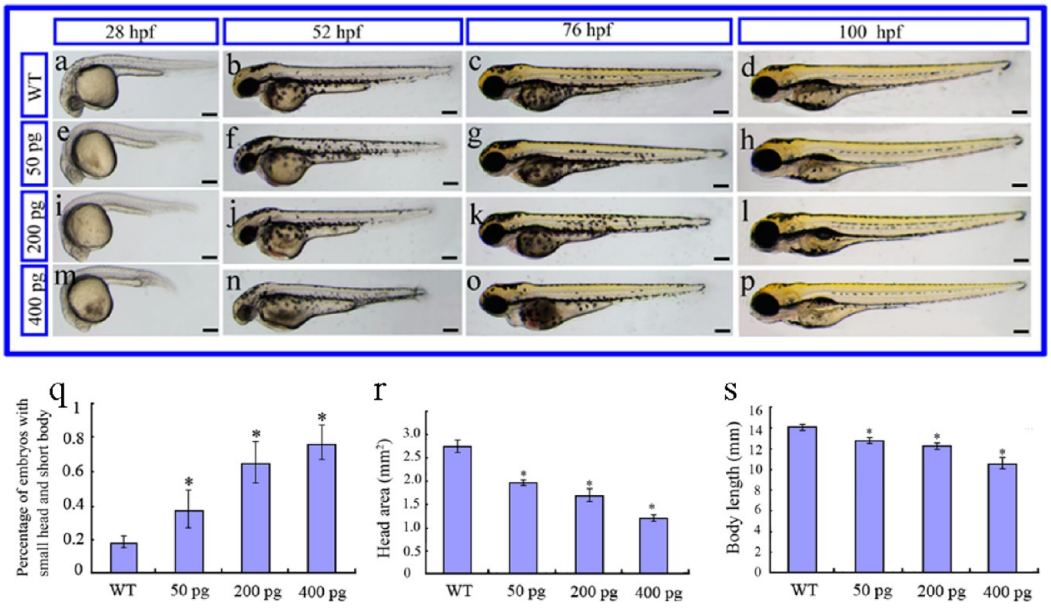

Figure 2. Phenotypes of embryos injected with different concentrations of BACP-2. (a−d) Morphological characteristics of uninjected embryos; (e−h) morphological characteristics of embryos that were injected with 50 pg of BACP-2; (i−l) morphological characteristics of embryos that were injected with 200 pg of BACP-2; (m−p) morphological characteristics of embryos injected with 400 pg of BACP-2. (q) Percentages of embryos with a small head and short body at 28 hpf in uninjected embryos and embryos injected with 50 pg of BACP-2, 200 pg of BACP-2, or 400 pg of BACP-2; (r) statistical analysis for the head region of uninjected embryos and embryos that were injected with BACP-2. (s) Statistical analysis of the body lengths of uninjected embryos and embryos injected with BACP-2. The data are presented as the mean ± SEM. * indicates a significant difference from the control group ($P < 0.05$). Scale bars = 200 μm.

dx.doi.org/10.1021/tx3004032 | Chem. Res. Toxicol. 2013, 26, 89−95

At 6 hpf, 93% of uninjected embryos were at the shield stage, while the embryos injected with BACP-2 were somewhat delayed. The percentages of embryos at the shield stage were 73%, 73%, and 16% in the groups injected with 50 pg, 200 pg, and 400 pg of BACP-2, respectively. The remaining embryos in each group were at 50% epiboly (Figure 3a). As epiboly continued, 67% of the uninjected embryos were at 90% epiboly at 8.5 hpf, while the percentage of embryos at 90% epiboly ranged from 62% in the 50 pg group to 45% in the 400 pg group. The number of embryos at 70%−80% epiboly increased as the injected concentration of BACP-2 increased (Figure 3b). The number of embryos at bud stage decreased as the amount of BACP-2 injected in each embryo increased, and the remaining embryos in each group were at 80%−90% epiboly (Figure 3c). These data indicate that BACP-2 injection led to developmental retardation in a concentration-dependent manner during the process of epiboly.

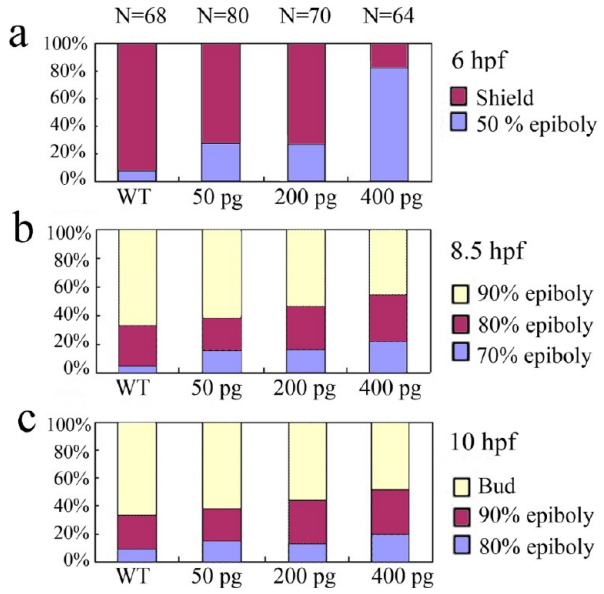

Figure 3. BACP-2 injection causes early developmental delay in zebrafish. (a) Percentages of embryos at different stages at 6 hpf; (b) percentages of embryos at different stages at 8.5 hpf; (c) percentages of embryos at different stages at 10 hpf.

In addition, we performed alcian blue staining in uninjected embryos and embryos injected with 50 pg, 200 pg, and 400 pg BACP-2 at 5 dpf to examine their cartilage development. No difference was observed between the four groups (Figure 4 and Figure S1, Supporting Information), which suggests that BACP-2 had no effect on cartilage development.

Gene Expression Patterns of Embryos Injected with BACP-2. BACP-2 caused morphological defects in the head and the heart. During early development, cell movement and cell fate determination are crucial for body plan and pattern formation. Early cell movement and cell fate determination can be examined by detecting the gene expression pattern, which is regulated by a combination of signaling pathways. To determine if the effects of BACP-2 on the head and heart were due to abnormal cell movement or cell fate determination, we examined the expressions of genes involved in head and heart development in embryos injected with 400 pg of BACP-2 and in uninjected embryos. *krox20* (also known as Egr2) is a transcription factor that is involved in vertebrate hindbrain segmentation, particularly in the formation and specification of rhombomeres (r) 3 and 5.[27−29] The expression of *krox20* in r3 and r5 was identical in embryos injected with BACP-2 and in uninjeted embryos, but the area between r3 and r5 was narrow in all embryos injected with 400 pg of BACP-2 (Figure 5a,b and Figure S2, Supporting Information), indicating that BACP-2 injection could cause a decrease in the size of the hindbrain. *otx2* is known for its central function as a transcriptional regulator in the development of the forebrain and midbrain in vertebrates.[30,31] The expression of *otx2* in 80% of embryos injected with 400 pg of BACP-2 was different from that in uninjected embryos (Figure 5c,d and Figure S3, Supporting Information). The abnormal expression of *otx2* in BACP-2-treated embryos suggests that the small-eyes phenotype observed in embryos injected with BACP-2 was related to the abnormal expression of *otx2*, which is also involved in eye development such as retinal pigment epithelium specification and photoreceptor cell fate determination.[32,33] Cardiac myosin light chain 2 (*cmlc2*), which is an essential component of the thick myofilament assembly and contractility of the heart, has frequently been used as a heart-specific marker.[34−36] The heart was located in the middle of the body at 24 hpf in 72% of embryos injected with 400 pg of BACP-2, while the heart was located on the left side of the body in all uninjected embryos (Figure 5e,f and Figure S4, Supporting Information). At 33 hpf, *cmlc2* expression revealed that the heart was located on the right side of the body in approximately 20% of embryos injected with 400 pg of BACP-2 (Figure 5g,h and Figure S5, Supporting Information). The expression of *cmlc2* in BACP-2-injected embryos demonstrated that BACP-2 affected heart development in zebrafish embryos. Overall, the gene expression

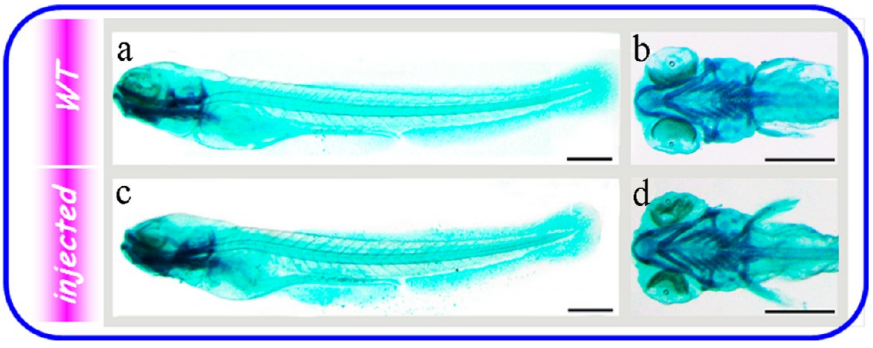

Figure 4. Effect of 400 pg of BACP-2 on cartilage development dectected by alcian blue staining at 5 dpf. (a,c) Lateral view with the anterior to the left. (b,d) Ventral view of the pharyngeal cartilage. Scale bars = 500 μm.

dx.doi.org/10.1021/tx3004032 | *Chem. Res. Toxicol.* 2013, 26, 89−95

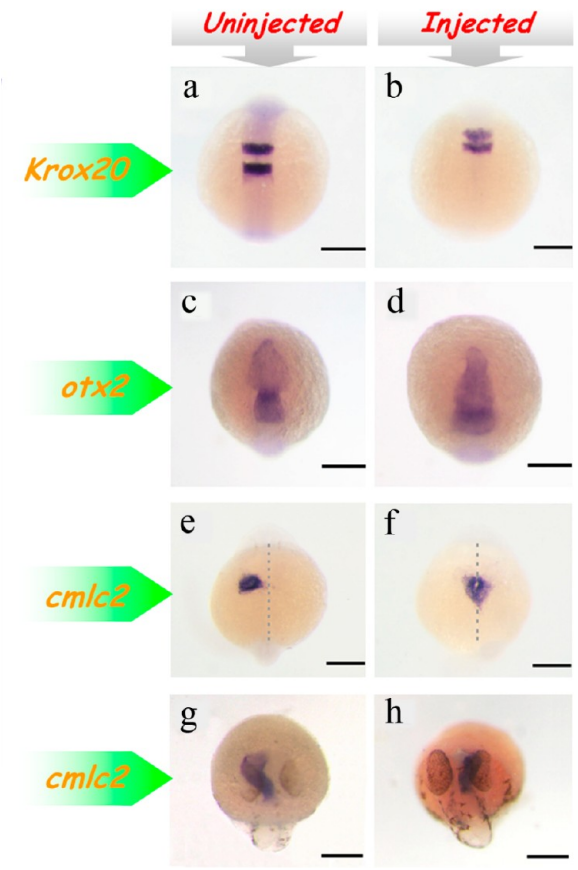

Figure 5. Expression of genes in embryos injected with 400 pg of BACP-2 and uninjected embryos. (a–h) Dorsal view. (a,b) Expression of krox20 at 12 hpf; (c,d) expression of otx2 at 12 hpf; (e,f) expression of cmlc2 at 24 hpf; (g,h) expression of cmlc2 at 33 hpf. Scale bars = 200 μm.

profile indicated that BACP-2 had detrimental effects on embryonic head and heart development that were related to alterations in gene expression, suggesting that BACP-2 exhibits some level of toxicity in early zebrafish embryos.

Epiboly delay is believed to be caused by a defect in cell migration during epiboly.[14,37] To determine if epiboly delay was related to a disorder of cell migration or to slow growth, we examined the expression of no tail (*ntl*) in embryos at 5.5 hpf, 8.5 hpf, and 10 hpf. No tail, a member of T-box transcription factor family,[38,39] is a marker for the induction of the mesoderm, which gives rise to posterior body structures, and was expressed in the margin, axial chordal mesoderm, and notochord during the development of uninjected embryos (Figures 6a, 7a, and 8a). The misexpression of *ntl* was associated with the abnormal migration of *ntl*-expressing cells. At 5.5 hpf, approximately 20% of embryos injected with 50 pg of BACP-2 expressed *ntl* at the site of 30% epiboly, which was similar to the normal expression of *ntl* at the 30% epiboly stage (4.7 hpf) (Figure 6b,d). When the injected amount of BACP-2 increased from 50 pg per embryo to 400 pg, the number of embryos with *ntl* expression at the site of 30% epiboly increased significantly, implying that the epiboly delay in these embryos was due to slow growth (Figure 6b,d). At 5.5 hpf, the abnormal expression of *ntl* in some embryos in each injected group manifested in a wave shape (Figure 6c,d), demonstrating that the epiboly delay was caused by abnormal cell migration in these embryos.

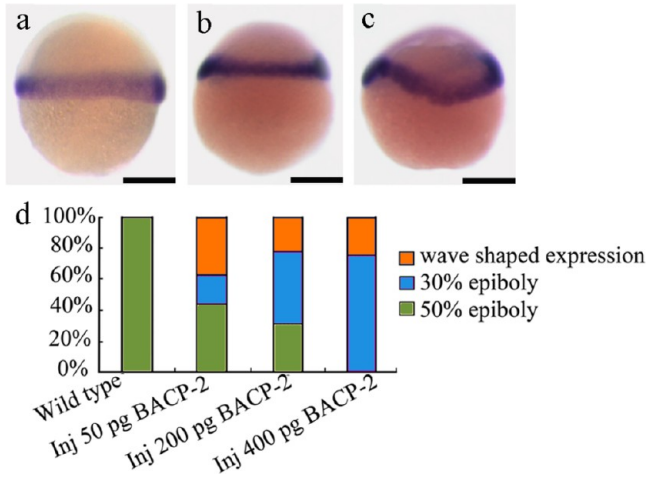

Figure 6. Expression of *ntl* at 5.5 hpf in the uninjected group and groups injected with 50 pg, 200 pg, or 400 pg of BACP-2. (a) Normal expression of *ntl* at the site of 50% epiboly. (b) Expression of *ntl* at the site of 30% epiboly. (c) Expression of *ntl* in a wave shape. (d) Statistical analysis of three types of *ntl* expression at 5.5 hpf in four groups. Scale bars = 200 μm.

As uninjected embryos developed to the stage of 80% epiboly, approximately 40% of the embryos in groups treated with 50 pg or 200 pg of BACP-2 exhibited abnormal slanted expression of *ntl* in the axial chordal mesoderm (Figure 7c,e),

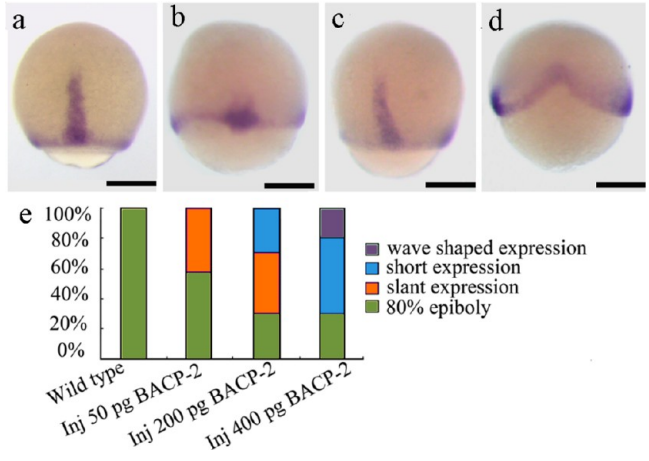

Figure 7. Expression of *ntl* at 8 hpf in the uninjected group and groups injected with 50 pg, 200 pg, and 400 pg of BACP-2. (a) Expression of *ntl* at the 80% stage of epiboly. (b) Reduced expression of *ntl* in the axial chordal mesoderm. (c) Slanted expression of *ntl* in the axial chordal mesoderm. (d) Expression of *ntl* in a wave shape. (e) Statistical analysis of four types of *ntl* expression at 8 hpf in four groups. Scale bars = 200 μm.

and some embryos (30% and 50%) with lower *ntl* expression in the axial chordal mesoderm were also observed in the 200 pg and 400 pg BACP-2-injected groups (Figure 7b,e). In 20% of embryos injected with 400 pg of BACP-2, abnormal wave-shaped *ntl* expression also appeared at the 80% epiboly stage (Figure 7d,e). At 10 hpf, slightly lower *ntl* expression in the axial chordal mesoderm was observed in the 50 pg- and 400 pg-injected groups (Figure 8b,d), which was similar to the expression at 90% epiboly, again implying that the observed epiboly delay in these embryos was due to slow growth. Slanted expression in the axial chordal mesoderm and unclosed looped

dx.doi.org/10.1021/tx3004032 | *Chem. Res. Toxicol.* 2013, 26, 89–95

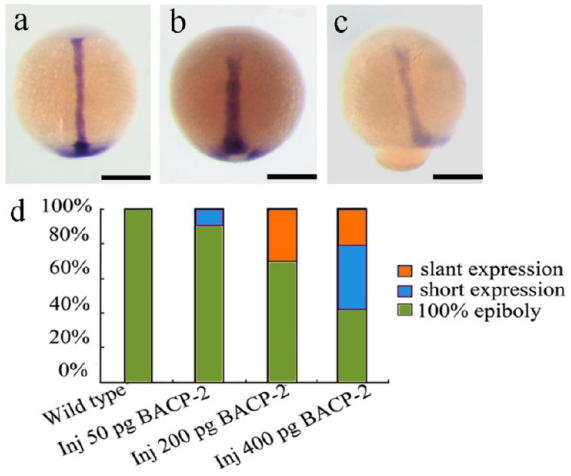

Figure 8. Expression patterns of *ntl* at 10 hpf in the uninjected group and in the groups injected with 50 pg, 200 pg, or 400 pg of BACP-2. (a) Normal expression of *ntl* in embryos at 10 hpf. (b) Slightly reduced expression of *ntl* in the axial chordal mesoderm. (c) Slanted expression of *ntl* in the axial chordal mesoderm and unclosed looped expression of *ntl* in the margin. (d) Statistical analysis of the four types of *ntl* expression at 10 hpf in the four groups. Scale bars = 200 μm.

expression in the margin appeared in the 200 pg- and 400 pg-injected groups (Figure 8c,d). The misexpression of *ntl* at three stages in embryos injected with BACP-2 demonstrates that the epiboly delay in these embryos was due to abnormal cell migration during the epiboly process. Overall, the expression of *ntl* during epiboly demonstrates that the observed epiboly delay resulted from both the effect of BACP-2 on cell migration during gastrulation and from slow growth.

CONCLUSIONS

With the rapid development of nanotechnology, nanoparticles have been increasingly and widely applied in various fields, including photonics, catalysis, and medicine. The toxicity and biocompatibility of nanoparticles have become an important concern, particularly in nanomedicine. Bismuth complexes are used extensively to treat human gastric and duodenal ulcers, and thus, their toxicity must be addressed. In this study, we used zebrafish embryos as an animal model to evaluate the toxicity of BACP-2, a bismuth derivative, on morphology and gene expression. Our study demonstrated that BACP-2 injection at the 1−4 cell stage leads to the development of smaller heads (particularly the eyes), shorter body lengths, and pericardial edemas. The severity and occurrence of these phenotypes are significantly concentration-dependent. The expression levels of genes such as *krox20*, *otx2*, and *cmlc2* indicate that the effect of BACP-2 on the head and heart is related to an alteration in gene expression patterns. Epiboly delay was also observed, and the expression pattern of *ntl* suggests that the epiboly delay is caused by the effect of BACP-2 on cell migration and slow growth. These results indicate that BACP-2 exhibits concentration-dependent developmental toxicity, indicating that the toxicity of bismuth derivatives must be rigorously evaluated before their application in nanomedicine.

ASSOCIATED CONTENT

Supporting Information

Alcian blue stained results showing the effect of BACP-2 at different concentrations on cartilage development; statistical analysis of the expression of *krox20* in wild-type embryos and 400 pg of BACP-2-injected embryos; statistical analysis of expression of *otx2* in wild-type embryos and 400 pg of BACP-2-injected embryos; statistical analysis of expression of *cmlc2* in wild-type embryos and 400 pg of BACP-2-injected embryos at 24 hpf; and statistical analysis of expression of *cmlc2* in wild-type embryos and 400 pg of BACP-2-injected embryos at 33 hpf. This material is available free of charge via the Internet at http://pubs.acs.org.

AUTHOR INFORMATION

Corresponding Author

* Fax/Tel: +86 22 23507022. E-mail: chendy@nankai.edu.cn (D.C.); xzfeng@nankai.edu.cn (X.F.).

Author Contributions

N.H. and X.L. contributed equally to this work.

Funding

This work was supported by the National Natural Science Foundation of China (81071260 and 61127006), the Doctoral Fund of the Ministry of Education of China (20100031120045), and the Tianjin Science Technology Research Funds of China (10JCZDJC17000 and 10JCYBJC25300).

Notes

The authors declare no competing financial interest.

ACKNOWLEDGMENTS

We thank Professor Hongwei Zhang of Shandong University for the gift of plasmids containing *ntl*, *krox20*, *otx2*, and *cmlc2* fragments. We thank Jianlin Cui of Nankai University for caring for the zebrafish.

ABBREVIATIONS

BACP-2, bismuth−asparagine coordination polymer spheres; *ntl*, no tail; *cmlc2*, cardiac myosin light chain 2; *otx2*, orthodenticle homeobox 2

REFERENCES

(1) Caruthers, S. D., Wickline, S. A., and Lanza, G. M. (2007) Nanotechnological applications in medicine. *Curr. Opin. Biotechnol. 18* (1), 26−30.

(2) Kurath, M., and Maasen, S. (2006) Toxicology as a nano-science?−disciplinary identities reconsidered. *Part. Fibre Toxicol. 3* (6), 1−13.

(3) deKrafft, K. E., Xie, Z., Cao, G., Tran, S., Ma, L., Zhou, O. Z., and Lin, W. (2009) Iodinated nanoscale coordination polymers as potential contrast agents for computed tomography. *Angew. Chem., Int. Ed. 48* (52), 9901−9904.

(4) Rieter, W. J., Pott, K. M., Taylor, K. M., and Lin, W. (2008) Nanoscale coordination polymers for platinum-based anticancer drug delivery. *J. Am. Chem. Soc. 130* (35), 11584−11585.

(5) Oh, M., and Mirkin, C. A. (2006) Ion exchange as a way of controlling the chemical compositions of nano- and microparticles made from infinite coordination polymers. *Angew. Chem., Int. Ed. 45* (33), 5492−5494.

(6) Kinsella, J. M., Jimenez, R. E., Karmali, P. P., Rush, A. M., Kotamraju, V. R., Gianneschi, N. C., Ruoslahti, E., Stupack, D., and Sailor, M. J. (2011) X-ray computed tomography imaging of breast

cancer by using targeted peptide-labeled bismuth sulfide nanoparticles. *Angew. Chem., Int. Ed. 50* (51), 12308−12311.
(7) Sun, H., Zhang, L., and Szeto, K. Y. (2004) Bismuth in medicine. *Met. Ions Biol. Syst. 41*, 333−78.
(8) Tsang, C. N., Ho, K. S., Sun, H., and Chan, W. T. (2011) Tracking bismuth antiulcer drug uptake in single *Helicobacter pylori* cells. *J. Am. Chem. Soc. 133* (19), 7355−7357.
(9) Yang, N., Tanner, J. A., Wang, Z., Huang, J. D., Zheng, B. J., Zhu, N., and Sun, H. (2007) Inhibition of SARS coronavirus helicase by bismuth complexes. *Chem. Commun. (Cambridge, U.K.)*. No. 42, 4413−4415.
(10) Chen, R., Gao, C. Y., Wu, Y. P., Wang, H., Zhou, H., Liu, Y., Sun, P., Feng, X. Z., and Chen, T. H. (2011) Facile synthesis of functional bismuth-amino acid coordination polymer nano-structures. *Chem. Commun (Cambridge, U.K.). 47* (28), 8136−8138.
(11) Luo, Y., Wang, C. M., Qiao, Y., Hossain, M., Ma, L. Y., and Su, M. (2012) In vitro cytotoxicity of surface modified bismuth nanoparticles. *J. Mater. Sci. Mater. Med. 23* (10), 2563−2573.
(12) Lepage, S. E., and Bruce, A. E. (2010) Zebrafish epiboly: mechanics and mechanisms. *Int. J. Dev. Biol. 54* (8−9), 1213−1228.
(13) Tada, M., and Kai, M. (2009) Noncanonical Wnt/PCP signaling during vertebrate gastrulation. *Zebrafish 6* (1), 29−40.
(14) Weijer, C. J. (2009) Collective cell migration in development. *J. Cell Sci. 122* (Pt 18), 3215−3223.
(15) Wheeler, G. N., and Brandli, A. W. (2009) Simple vertebrate models for chemical genetics and drug discovery screens: lessons from zebrafish and Xenopus. *Dev. Dyn. 238* (6), 1287−1308.
(16) Patton, E. E., and Zon, L. I. (2001) The art and design of genetic screens: zebrafish. *Nat. Rev. Genet. 2* (12), 956−966.
(17) Kane, D. A., Hammerschmidt, M., Mullins, M. C., Maischein, H. M., Brand, M., van Eeden, F. J., Furutani-Seiki, M., Granato, M., Haffter, P., Heisenberg, C. P., Jiang, Y. J., Kelsh, R. N., Odenthal, J., Warga, R. M., and Nusslein-Volhard, C. (1996) The zebrafish epiboly mutants. *Development 123*, 47−55.
(18) Karlstrom, R. O., Tyurina, O. V., Kawakami, A., Nishioka, N., Talbot, W. S., Sasaki, H., and Schier, A. F. (2003) Genetic analysis of zebrafish gli1 and gli2 reveals divergent requirements for gli genes in vertebrate development. *Development 130* (8), 1549−1564.
(19) Fako, V. E., and Furgeson, D. Y. (2009) Zebrafish as a correlative and predictive model for assessing biomaterial nanotoxicity. *Adv. Drug Delivery Rev. 61* (6), 478−486.
(20) Hill, A. J., Teraoka, H., Heideman, W., and Peterson, R. E. (2005) Zebrafish as a model vertebrate for investigating chemical toxicity. *Toxicol. Sci. 86* (1), 6−19.
(21) Wang, Y., Seebald, J. L., Szeto, D. P., and Irudayaraj, J. (2010) Biocompatibility and biodistribution of surface-enhanced Raman scattering nanoprobes in zebrafish embryos: in vivo and multiplex imaging. *ACS Nano 4* (7), 4039−4053.
(22) Liu, Y., Liu, B., Feng, D. F., Gao, C. Y., Wu, M., He, N. N., Yang, X. L., Li, L., and Feng, X. Z. (2012) A progressive approach on zebrafish toward sensitive evaluation of nanoparticles' toxicity. *Integr. Biol. 4* (3), 285−291.
(23) Lee, K. J., Nallathamby, P. D., Browning, L. M., Osgood, C. J., and Xu, X. H. (2007) In vivo imaging of transport and biocompatibility of single silver nanoparticles in early development of zebrafish embryos. *ACS Nano 1* (2), 133−143.
(24) Westerfield, M. (2007) The zebrafish book: a guide for the laboratory use of zebrafish *Danio (Brachydanio) rerio*, http://zfin.org/zf_info/zfbook/zfbk.html.
(25) Shao, J., Chen, D., Ye, Q., Cui, J., Li, Y., and Li, L. (2011) Tissue regeneration after injury in adult zebrafish: the regenerative potential of the caudal fin. *Dev. Dyn. 240* (5), 1271−1277.
(26) Walker, M. B., and Kimmel, C. B. (2007) A two-color acid-free cartilage and bone stain for zebrafish larvae. *Biotech. Histochem. 82* (1), 23−28.
(27) Labalette, C., Bouchoucha, Y. X., Wassef, M. A., Gongal, P. A., Le Men, J., Becker, T., Gilardi-Hebenstreit, P., and Charnay, P. (2011) Hindbrain patterning requires fine-tuning of early krox20 transcription by Sprouty 4. *Development 138* (2), 317−326.
(28) Borday, C., Chatonnet, F., Thoby-Brisson, M., Champagnat, J., and Fortin, G. (2005) Neural tube patterning by *Krox20* and emergence of a respiratory control. *Respir. Physiol. Neurobiol. 149* (1−3), 63−72.
(29) Chatonnet, F., Wrobel, L. J., Mezieres, V., Pasqualetti, M., Ducret, S., Taillebourg, E., Charnay, P., Rijli, F. M., and Champagnat, J. (2007) Distinct roles of *Hoxa2* and *Krox20* in the development of rhythmic neural networks controlling inspiratory depth, respiratory frequency, and jaw opening. *Neural Dev. 2*, 19.
(30) Spieler, D., Baumer, N., Stebler, J., Koprunner, M., Reichman-Fried, M., Teichmann, U., Raz, E., Kessel, M., and Wittler, L. (2004) Involvement of Pax6 and Otx2 in the forebrain-specific regulation of the vertebrate homeobox gene ANF/Hesx1. *Dev. Biol. 269* (2), 567−579.
(31) Scholpp, S., Foucher, I., Staudt, N., Peukert, D., Lumsden, A., and Houart, C. (2007) Otx1l, Otx2 and Irx1b establish and position the ZLI in the diencephalon. *Development 134* (17), 3167−3176.
(32) Nishihara, D., Yajima, I., Tabata, H., Nakai, M., Tsukiji, N., Katahira, T., Takeda, K., Shibahara, S., Nakamura, H., and Yamamoto, H. (2012) Otx2 is involved in the regional specification of the developing retinal pigment epithelium by preventing the expression of sox2 and fgf8, factors that induce neural retinal differentiation. *PLoS One 7* (11), e48879.
(33) Muranishi, Y., Terada, K., Inoue, T., Katoh, K., Tsujii, T., Sanuki, R., Kurokawa, D., Aizawa, S., Tamaki, Y., and Furukawa, T. (2011) An essential role for Rax homeoprotein and NOTCH-HES signaling in Otx2 expression in embryonic retinal photoreceptor cell fate determination. *J. Neurosci. 31* (46), 16792−16807.
(34) Rottbauer, W., Wessels, G., Dahme, T., Just, S., Trano, N., Hassel, D., Burns, C. G., Katus, H. A., and Fishman, M. C. (2006) Cardiac myosin light chain-2: a novel essential component of thick-myofilament assembly and contractility of the heart. *Circ. Res. 99* (3), 323−331.
(35) Zhao, L., Zhao, X., Tian, T., Lu, Q., Skrbo-Larssen, N., Wu, D., Kuang, Z., Zheng, X., Han, Y., Yang, S., Zhang, C., and Meng, A. (2008) Heart-specific isoform of tropomyosin4 is essential for heartbeat in zebrafish embryos. *Cardiovasc. Res. 80* (2), 200−208.
(36) Xu, D. J., Bu, J. W., Gu, S. Y., Xia, Y. M., Du, J. L., and Wang, Y. W. (2011) Celecoxib impairs heart development via inhibiting cyclooxygenase-2 activity in zebrafish embryos. *Anesthesiology 114* (2), 391−400.
(37) Loucks, E. J., and Ahlgren, S. C. (2009) Deciphering the role of Shh signaling in axial defects produced by ethanol exposure. *Birth. Defects Res., Part A. 85* (6), 556−567.
(38) Pei, D. S., Sun, Y. H., Long, Y., and Zhu, Z. Y. (2008) Inhibition of no tail (*ntl*) gene expression in zebrafish by external guide sequence (EGS) technique. *Mol. Biol. Rep. 35* (2), 139−143.
(39) Marlow, F., Gonzalez, E. M., Yin, C., Rojo, C., and Solnica-Krezel, L. (2004) No tail co-operates with non-canonical Wnt signaling to regulate posterior body morphogenesis in zebrafish. *Development 131* (1), 203−216.